UNIVERSITY OF
BATH

University of Bath

Effectiveness of Superconducting Fault Current Limiting Transformers in Power Systems

M. Elshiekh, M. Zhang, Harsha Ravindra, Xi Chen, Sriharsha Venuturumilli, Xiaohua Huang, Karl Schoder, Mischa Steurer, W. Yuan

Abstract—**Superconducting devices have emerged in many applications during the last few decades. They offer many advantages including high efficiency, compact size, and superior performance. However, the main drawback of these devices is the high cost. An option to reduce the high cost and improve the cost-benefit ratio is to integrate two functions into one device. This paper presents the superconducting fault current limiting transformer (SFCLT) as a superior alternative to normal power transformers. The transformer has superconducting windings and also provides fault current limiting capability to reduce high fault currents. The SFCLT is tested in two power system models: a 7 bus wind farm based model simulated in PSCAD and on the 80 bus simplified Australian power system model simulated in RTDS. Various conditions were studied to investigate the effectiveness of the fault current limiting transformer.**

Index Terms— **Transformers, superconducting, fault current limiters .**

I. INTRODUCTION

TRANSFORMERS have evolved considerably in the last few decades, reaching efficiencies of up to 99%. Yet, for high power ratings, conventional power transformers are still very bulky, costly, and sensitive to fault currents. With the ever-increasing power demands and the lack of sufficient space to install additional substations or upscale existing ones in densely populated areas, the power densities must be increased.

In addition, short circuit current levels continue to rise due to increased network power capacity. This problem has a significant effect, especially in networks containing wind power generation. In the past, the major concern was related to the wind turbines itself. During grid disturbances, the wind turbines are generally tripped to avoid damaging them. However, with the increase in wind turbine generation, loss of generation from these units following a network disturbance has an adverse impact on network stability. As such, keeping wind turbines connected to the grid while protecting the generators from high fault currents is an important issue. The fault current level may be decreased by the high impedance of the conventional power transformers during normal operation. However, this can cause increasing the impedance of a transformer to reach 20% [1], which decreases the transmission efficiency during normal operation.

Inserting superconducting fault current limiters (SFCL) next to the conventional transformer could be a nice solution, which helps in achieving fault tolerant performance and reduced losses in steady-state conditions [2], [3]. However, this solution requires additional devices, which incurs additional cost and space and, therefore, not alleviating the constraints imposed by the conventional bulky transformers. High temperature superconducting (HTS) transformers have been proposed to deal with high power densities by lowering the losses in the transmission system and with a more compact design than normal power transformers with similar rating [4], [5]. On the other hand, HTS transformers offer reduced impedance than conventional transformers, but having the advantage of a much smaller footprint and fault current limiting function, i.e. SFCLT's [6], [7].

Installing SFCLT's can achieve low impedance during steady-state operation in addition to suppressing fault currents to lower levels, protecting the system and achieving more stable operation during and after faults. SFCLTs are much similar to normal transformers in construction but do have superconducting windings in place of copper windings. During fault conditions, the superconducting windings quench and the resulting high resistance path helps in reducing the fault current magnitude.

In this paper, two power system models and several fault scenarios are presented to demonstrate that adding SFCLT at strategic locations in a power system improves stability. A 100 MVA SFCLT is used in the first power system example to connect combined diesel and wind generation to the grid as shown in Figure 1. In the second example, two 370 MVA SFCLTs are replacing conventional transformers in a simplified Australian power system model.

Firstly, the 100 MVA SFCLT transformer design is introduced based on an existing 100 MVA normal transformer [8]. Then, the application system examples are used within the electromagnetic transient-type software to study the effectiveness of the SFCLT in reducing fault currents in different scenarios, protecting the system elements and aiding in system stability.

II. Transformer Design

In light of the typical requirement for transformers at the transmission level, a 100 MVA class transformer design study was conducted. Table I provides the design target and general parameters of the HTS transformer proposed. The design of the 370 MVA SFCLT presented for case studies in the Australian power system model follows the design guidelines provided for the 100 MVA design.

TABLE I
100 MVA HTS TRANSFORMER DESIGN DATA

Rating	100 MVA
Type	3 phase transformer
Rated voltage	154 / 22.9 kV
Current	0.37 / 2.5 kA
Iron core	1.4 T
Frequency	50 Hz
Cooling	LN2
% Leakage Impedance	10%-15%
Estimated dimension	7.6 m × 5 m × 2.5 m
Weight	< 35 ton

For the design of the HTS transformer, the critical current of the second generation coated conductor is about 300 A/cm at 77 K [9]. The perpendicular component of the magnetic field at the coil ends is estimated to be 0.18 T, which could reduce the critical current of the second generation (2G) HTS tapes to 200 A/cm. In order to take the large operating current, several 2G HTS tapes must be connected in parallel. The minimum tape length is determined by the maximum endurable quenching voltage of 2G HTS. Assuming the transformer must withstand 200 msec. of fault duration and a peak voltage per unit length of 0.595 V/cm [10], the minimum lengths of the primary and secondary windings are 2.6 km and 385 m, respectively. For the primary winding current of 370 A, 8 tapes are connected in parallel based on the assumption that the maximum magnetic field to be reached is 1 T and the critical current of a single tape under 1 T is about 50 A. The same principle applies to the secondary winding, which requires 50 tapes in parallel. For the primary, each winding element has the 8 tapes connected in parallel with 215 turns in the axial direction and 15 turns in radial direction. In total, there are 3255 turns for the primary winding. The winding height is about 1 m when considering 1 mm between each element. The winding thickness is 0.04 m when considering 0.25 mm thickness for each tape with insulation.

For the secondary winding, there are 240 turns in the axis direction and 2 turns in the radial direction for a total of 480 turns. The winding height is about 1.212 m, considering 1 mm gap between each element. The winding thickness is 0.025 m, considering 0.25 mm thickness for each tape with insulation. The winding parameters are summarized in Table II.

The cost of the HTS windings is calculated based on 30 $/m. Comparing this cost to normal power transformer cost indicates that these transformers will not add a big difference in total costs. Normal transformers in the range 75-500 MVA cost about from $2 to $7.5 million in the United States [19]. This cost without transportation, taxes and other variable costs.

TABLE II
100 MVA HTS WINDING PARAMETERS

HTS PROPERTY	YBCO COATED CONDUCTOR
Thickness	0.1 mm
Width	4 mm
Stabilizer	Copper, 40 μm
Hastelloy Substrate	60 μm
Critical current	50 A
Primary winding	8 tapes in parallel, 2.6 km minimum length
Secondary	50 tapes in parallel, 385 m minimum length
Total HTS length for primary	20.8 km
Total HTS length for secondary	19 km
Estimated cost for HTS windings	$ 1.2 M

III. Modelling SFCLT's

A standard transformer model is used with series connected impedances representing the primary and secondary windings. Both sides are assumed to be superconducting windings. Copper is used as a stabilizer and tapes are connected in parallel according to the critical current of the superconducting material.

The winding series impedances consist of resistance (Rp and Rs) and leakage reactance (Xp and Xs). Whereas the resistance depends on the type of material used, the reactance depends on the design of the transformer. In the case of superconducting transformers under normal operating conditions, winding resistance values will be negligible.

For superconducting transformers using HTS tapes with a stabilizing layer, under fault conditions, the resistance of the windings will be defined by the resistance offered by the stabilizing layer as the superconducting layer gets quenched. Hence the impedance value will increase significantly, which in turn will decrease the amplitude of the fault current.

The main parameters that define the modes of operation of the SFCLT are the critical current density (J_c) and critical temperature (T_c). According to these values, the mode of operation of the superconducting element is determined. So, firstly, the critical current and the winding temperature must be calculated. The windings temperature mainly depends on the cooling system parameters and efficiency to reduce the power dissipated in the HTS windings.

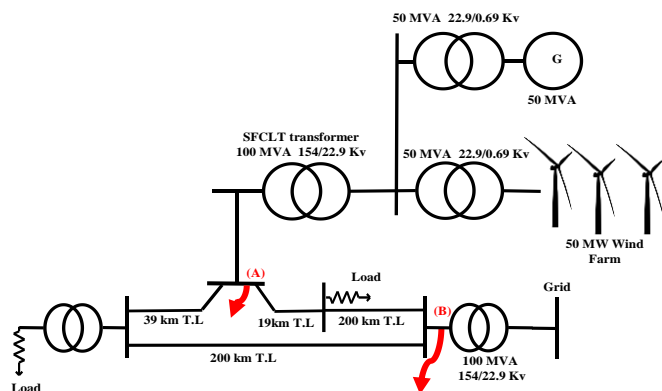The power dissipated in the superconducting material (P_{diss}) can be calculated by

Fig.1. Test system 1: Generation integration with fault current limiting HTS transformers.

$$P_{diss}(t) = i(t)^2 R_{sc}(t) \tag{1}$$

With R_{SC} is the total resistance of the superconducting windings, $i(t)$ is the current in the windings. The cooling power and energy absorbed by the cooler—which reduce the temperature rise during and after a fault—are calculated by

$$P_{\text{cooling}}(t) = hA(T(t) - 77) \tag{2}$$

Where h is heat transfer coefficient, which depends on the temperature rise, A is the surface area covered by the liquid nitrogen, and $T(t)$ is the winding temperature. The heat transfer coefficient (h) changes with the increase in the windings temperature. It represents the key factor in the recovery period which means returning to superconducting state after the quench. To consider the impact of the recovery period, the heat coefficient equations were taken from [11] as a function of the temperature rise. The assumption here is that the whole HTS windings are fully covered by liquid nitrogen during the quench process. The corresponding net power in the windings (P_{SC}) is the difference between the dissipated and cooling power. Then, the temperature of the windings can be calculated through

$$T(t) = T_o + \frac{1}{C_p} \int_0^t P_{SC}(t) \, dt \tag{3}$$

Where T_o be the initial temperature of the material, which is taken as 77 K and C_p (J/K) is the heat capacity of the material which represents the number of joules generated per each Kelvin degree. This amount depends on the specific heat capacity and the mass of the material. As the volume and specific heat capacity of each material in the tape are different, the heat capacity of each material is calculated individually by multiplying its specific heat value by the volume and the density of the material [12].

The heat capacity variation of the YBCO with temperature is approximated by the linear equation (4) for simplification.

$$C_{p(ybco)} = 2T \times d \times V \tag{4}$$

Where T is the temperature, d is the density of the material, and V is the volume. The copper heat capacity variation with the temperature is small so, it is neglected here while the substrate heat capacity can be calculated similarly to the YBCO material from (4). After this step, the total heat capacity is calculated by adding the three values of the three materials together.

The critical current density at which quenching occurs is calculated according to the following relation [13]:

$$J_c(T) = J_{co}\left(\frac{(T_c - T(t))^\alpha}{(T_c - T_o)^\alpha}\right) \tag{5}$$

Where J_{c0} is the critical current density at the initial temperature T_0, α is the density exponent and equal to 1.5, and T_c is the critical temperature; (5) is valid for $T < T_C$.

As $J_c(T)$ is less than the critical value specified for the material, the windings represent zero resistance and, therefore, the winding resistance will be neglected during normal operation. When the current passing through the transformer windings exceeds the critical current, the winding resistivity starts to increase according to the following equation:

$$\rho_{\text{HTS}} = \frac{E_c}{J_c(T)}\left(\frac{J}{J_c(T)}\right)^{n-1} T < T_c, J > J_c \tag{6}$$

When the temperature reaches its critical value, it will be in the normal resistive mode. During normal mode, the value of the resistance is only determined by the value of the stabilizer resistance because the superconducting material resistance becomes very high compared to the stabilizer resistance. The resistivity of the copper stabilizer is changed with the temperature according to this equation [14]:

$$\rho_{\text{cu}} = (0.0084T - 0.4603) \times 10^{-8}, T > T_c \tag{7}$$

Finally, from (6), (7) and the current $i(t)$ passing through it, the total resistance of the HTS winding R_{sc} is calculated.

IV. SMALL SCALE SYSTEM SIMULATION USING PSCAD

The first studied system (also referred to herein as TS1) consists of a combined diesel and wind farm generation unit of 50MW connected to the transmission system via the SFCLT as shown in Figure 1. All the components are modelled using PSCAD software [15].

The SFCLT is integrated with the grid to protect it from high fault currents and support system stability. Different fault types and locations are investigated to determine SFCLT and system behaviour. The results focus on the current limitation on both the primary and secondary sides of the transformer. Also, the temperature of both sides is studied, as it is an important parameter in designing the SFCLT and the cryogenic system.

To clarify the effectiveness of the SFCL on the current limitation, the circuit breakers are set to trip after 200ms. This time is chosen to allow the study of the SFCLT operation and the effect of its recovery time, in addition to considering circuit breakers failure to trip.

The simulation conditions have been tested for three scenarios; (a) single line to ground(S-L-G) fault at point A, (b) three-phase to ground (3-ph-G) fault at point A, and (c) single line
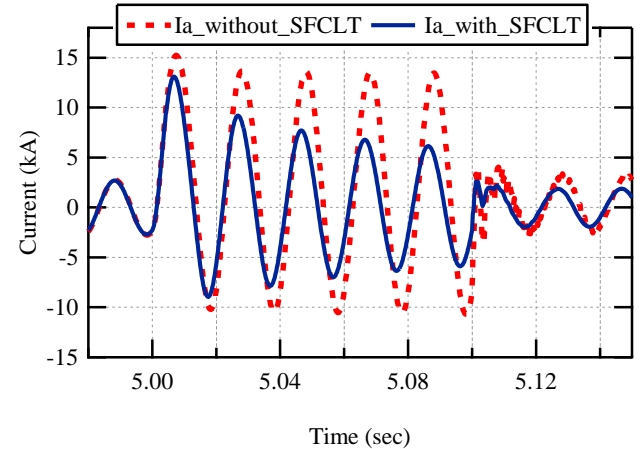

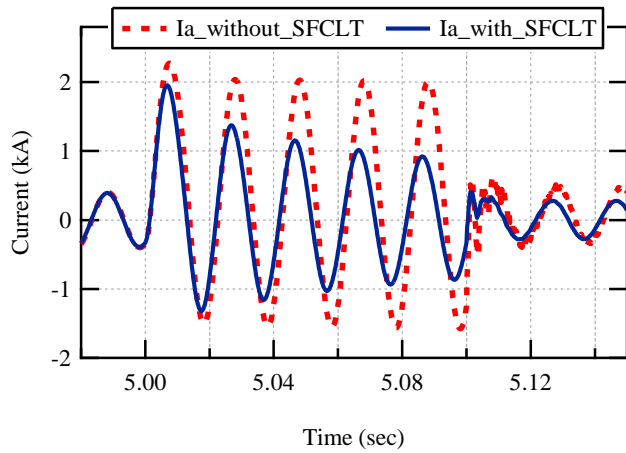Fig. 2. TS1–Case 1: Current at primary of SFCLT with S-L-G fault at A.

Fig. 3. TS1–Case1: Current at secondary of SFCLT with S-L-G fault at A.

to ground fault at point B. In all cases, the fault starts at second 5 and lasts for 100 msec. The simulation results of these conditions are discussed in the following.

1) TS1-CASE 1: S-L-G FAULT AT LOCATION A

Figure 2 and Figure 3 show currents at the primary and secondary winding of the SFCLT, respectively, when a single line-to-ground fault is applied at point A in Figure 1. From Figure 2, note that using SFCLT limits current at the first peak to about 12.7 kA from a prospective current of about 15.1 kA, 85% of the prospective value. Moreover, after the first peak, the percentage limitation increases and the current reaches 54% of the prospective values during the remaining fault period. The secondary side current is also reduced significantly, reaching about 1 kA during the fault period compared with 2 kA prospective value as shown in Figure 3, while the SFCLT limits the first peak to 86% from the prospective value. The temperature rise on both primary and secondary windings is shown in Figure 4. The maximum temperature during the fault on the primary side is 420 K while that on the secondary side is 350 K. The temperature rise value may be changed with different cooling methods. The windings take about 3.5 seconds to recover from the temperature rise and return to superconducting state. This recovery period has a minor effect on the transformer currents as shown in Figures 2
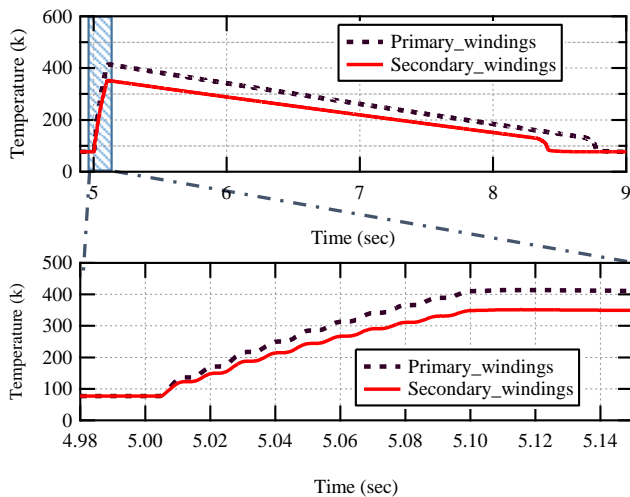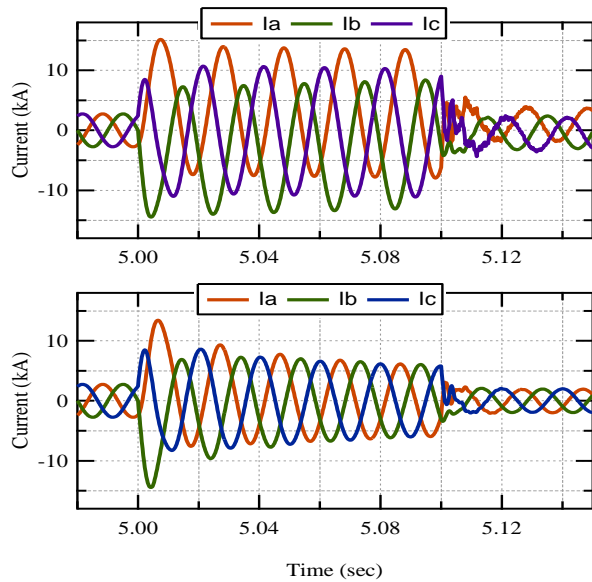

Fig. 5. TS1–Case 2: Currents at primary of SFCLT with 3-ph-G fault at C (a) without SFCLT, (b) with SFCLT.

and 3.

2) TS1-CASE 2: 3-PH-G FAULT AT LOCATION A

The second case tests a three phase to ground fault also at point A. The primary side currents without and with using the current limiting transformer are shown in Figure 5. The limitation of the three phase currents during the fault period was about 46% with a noticeable enhancement on the current transient period just after the fault clearance with using the SFCLT.

3) TS1-CASE 3: S-L-G FAULT AT LOCATION B

To further test the ability of the SFCLT to limit fault currents even if the fault location is far from the transformer location, a fault was applied at the grid terminals as shown in Figure 1. As the fault is more remote from the transformer location, the short circuit current value decreased slightly in this case. Figure 6 shows the current and temperature rise in the primary windings and the limitation in the first peak is less than 1 kA as the fault current is not very high in this case. However, the limitation increases during the fault to yield approximately 70% from the prospective current value. Also, the temperature on the primary side is less than 300K.
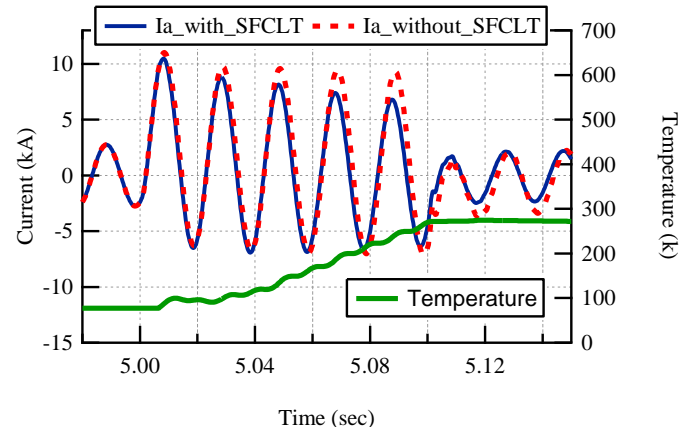

Fig. 4. TS1–Case1: Temperature at primary and secondary of SFCLT with fault at point A.

Fig. 6. TS1–Case 3: Current and Temperature at primary of SFCLT with fault at C.

V. LARGE SCALE SYSTEM MODELLING USING RTDS

A. SIMPLIFIED AUSTRALIAN POWER SYSTEM MODEL

The SFCLT model built in PSCAD was ported to the real time digital simulator RTDS™ [16] to allow study effects within a second but larger, multi-area power system (also referred to herein as TS2). The simplified Australian Power System model available in [17, 18] was modelled in electromagnetic transient type (EMTP) simulator, RTDS™ over 5 racks running in real-time at a 50 μs time step. The simplified Australian power system is a 29 GW, 50 Hz system with transmission voltage from 220–500 kV. Fourteen aggregated generation plants are modelled in five areas consisting of hydro,

steam and gas turbine based prime movers. The power flow transfer occurs from south to north (area 5 to area 2) as provided in Table III.

Area frequency control and inter-area power flow control is implemented in the system to maintain the desired inter-area power flow through area control error (ACE). Table IV provides data used for ACE control parameters.

B. APPLICATION OF SFCLT TO SUPPORT INCREASED POWER TRANSFERS

In the second system application, two transformers each rated 370 MVA between bus 315 (275 kV) and 308 (500 kV) were replaced by SFCLT. The base system can be seen in Fig-
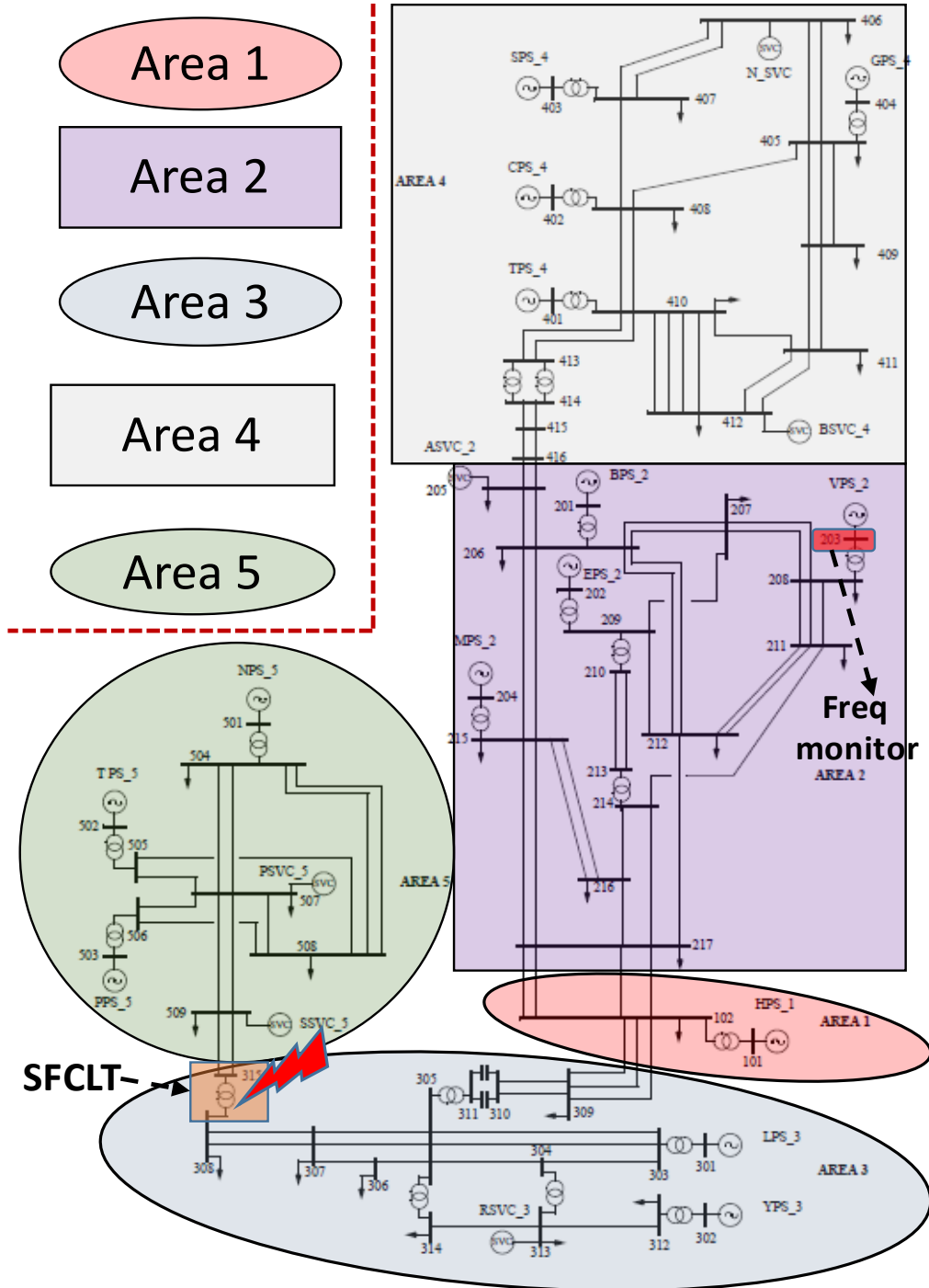

Fig. 7. Test system 2: Simplified Australian power system model.

ure 7, which only shows one of the transformers at this location. The SFCLT was designed and rated to handle appropriate voltage and current levels. See Figure 7 for the corresponding location of the replaced transformers. A three phase fault was applied at bus 315 with respect to phase A at 90 degree on the voltage waveform with a small impedance (0.01Ω) for 200 msec. Although faults in systems could be cleared in times as little as 50 msec, a duration of 200 msec was tested here to observe the system response in a limiting worst case scenario including the possibility of failing primary protection.

TABLE III
INTER-AREA POWER TRANSFER IN TS2 MODEL

From	To	MW
Area 5	Area 3	500
Area 3	Area 1	1000
Area 1	Area 2	1120
Area 2	Area 4	500

TABLE IV
ACE CONTROL PARAMETERS

Parameter	Value
kp	0.005
ki	0.05
B	-50MW/0.1 Hz

Figure 8 shows currents through one SFCLT between bus 315 and 308 and is compared with prospective fault currents in the case of a conventional transformer. It can be observed that the SFCLT limits the prospective fault current significantly. Though results of all areas and buses were examined, Bus 203 frequency excursions are shown in Figure 9 to demonstrate that a remote fault in Area 3 still causes a significant response from generators in Area 2. It can be observed that with the current limiting function provided by SFCLT, frequency excursions without SFCLT can reach around 380 mHz while with the SFCLT it is limited to ~110 mHz. The frequency as shown here is measured through a 3-phase phase locked loop, synchronous reference frame approach. Care has to be taken when drawing conclusions from frequency measurements as initial transients occur for typically half a fundamental cycle for symmetric faults and possibly up to the full fault duration in cases of asymmetric faults [20]. In addition, overshoot and oscillations in the estimated frequency will occur for some time after disturbance and fault events. For the automatic generation control, these transient conditions pose no issue. The test cases aimed at observing the system response and recovery for the same fault scenario while increasing inter-area power transfers from Area 5 to Area 3. The conclusion of a large set of the fault studies performed-while incrementally increasing power transfer from the1 initial 500 MVA-was that the fault limiting capability allows power transfers along the associated transmission lines of up to 650 MVA before a dynamic stability limit was reached.

Figure 10 shows rms-current trace examples as measured through transformer primary (Bus 315) for the three-phase fault with various inter-area exchange values. The current set-
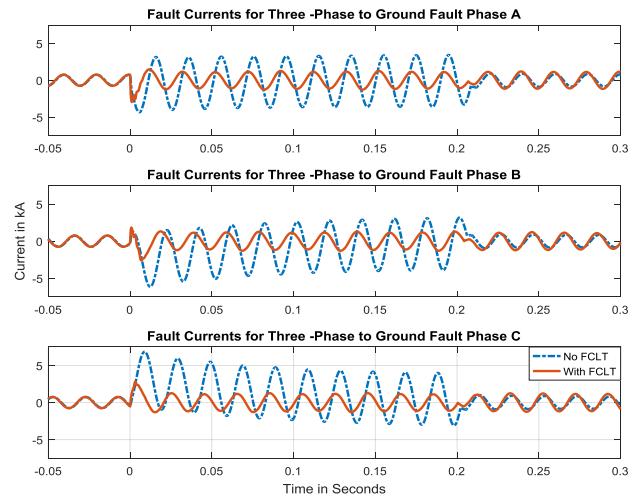

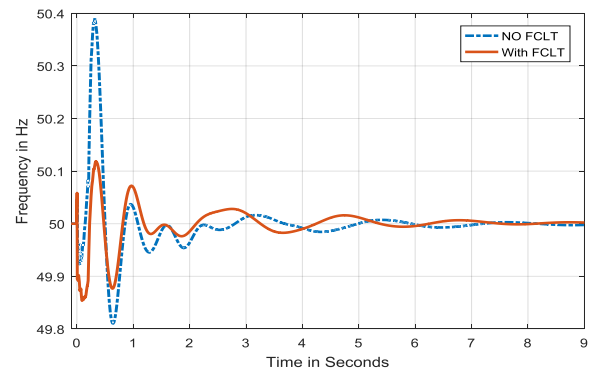Fig. 8. TS2: Currents through transformer at bus 315 for a three phase fault.

Fig. 9. TS2: Frequency at Bus 203 for a three phase fault.

tles and the system recovers until the inter-area flow is at 720 MW, with the current trace shown until about 2.2 seconds after disturbance initiation. Table V summaries conditions and response metric with varying inter-area power transfer values. The recovery time measures the time taken for the current through the transformer at Bus 315 to settle to within 5% of the pre-disturbance value.
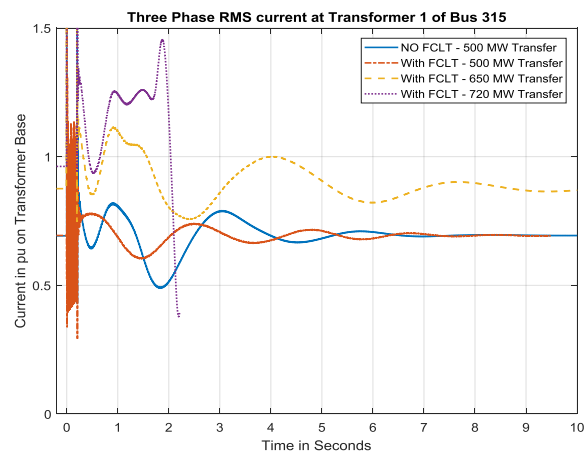

Fig.10.TS2: RMS current at BUS 315 for three phase fault with different inter-area power transfer values.

TABLE V
INTER-AREA POWER TRANSFER IN TS2 MODEL

Area 5 to Area 3 power flow (MW)	Recovery Time (s) (±5% Iinit)	Inter-Area power transfer state
500 – No SFCLT	3.45	Recovered
500 – SFCLT	2.43	Recovered
650 – SFCLT	5.48	Recovered
720 - SFCLT	--	Unstable

VI. CONCLUSION

The design and modelling presented herein allow to study in detail the current limiting behaviour of large superconducting fault current limiting transformers. Such SFCLTs may support, for example, interconnecting newly installed generation and increased power transfers with existing systems without the need to upgrade other infrastructure elements. In addition to the electrical behaviour, the studies presented herein consider the temperature rise of the superconducting winding during the quench, which is considered important with respect to the effectiveness of such high rating transformers.

The results obtained using the developed models prove that SFCLTs are able to provide significant benefits as compared with normal transformers. In the studies, fault currents could effectively and consistently be limited to lower values. Coordination with normal protection devices is possible. Frequency excursions observed in the system could also be reduced using the fault current limiting transformers, thereby helping improve stability characteristics. The fault currents are limited within the first cycle and continue to be held much lower values in subsequent fault periods.

REFERENCES

[1] N. Hayakawa, H. Kojima, M. Hanai and H. Okubo, "Progress in Development of Superconducting Fault Current Limiting Transformer (SFCLT)," in IEEE Transactions on Applied Superconductivity, vol. 21, no. 3, pp. 1397-1400, June 2011.

[2] M. E. Elshiekh, D. E. A. Mansour and A. M. Azmy, "Improving Fault Ride-Through Capability of DFIG-Based Wind Turbine Using Superconducting Fault Current Limiter," in IEEE Transactions on Applied Superconductivity, vol. 23, no. 3, pp. 5601204-5601204, June 2013.

[3] W. T. B. de Sousa, T. M. L. Assis, A. Polasek, A. M. Monteiro and R. de Andrade, "Simulation of a Superconducting Fault Current Limiter: A Case Study in the Brazilian Power System With Possible Recovery Under Load," in IEEE Transactions on Applied Superconductivity, vol. 26, no. 2, pp. 1-8, March 2016.

[4] Kim, Sung-Hoon, Woo-Seok Kim, Kyeong-Dal Choi, Hyeong-Gil Joo, Gye-Won Hong, Jin-Ho Han, Hee-Gyoun Lee, Jung-Ho Park, Hee-Suck

[5] Bohno, T., A. Tomioka, M. Imaizumi, Y. Sanuki, T. Yamamoto, Y. Yasujawa, H. Ono, Y. Yagi, and K. Iwadate. 2005. "Development of 66 kV/69 kV 2 MV A prototype HTS power transformer." Physica C, Super-conductivity 1402-1407.

[6] Ohtsubo, Y., et al. "Development of REBCO Superconducting Transformers with a Current Limiting Function - Fabrication and Tests of 6.9 kV-400 kVA Transformers." IEEE Transactions on Applied Superconductivity 25, no. 3 (June 2015): 1-5.

[7] Iwakuma, M., et al. "Development of a three phase 66/6.9 kV-2 MVA REBCO Superconducting Transformer." IEEE Transactions on Applied Superconductivity 25, no. 3 (June 2015): 1-6.

[8] Choi, J., Lee, S., Park, M., Kim, W., Kim, S., Han, J.Choi, K. (2007). Design of 154 kV class 100 MVA 3 phase HTS transformer on a common magnetic core. Physica C: Superconductivity and its Applications, 463-465(SUPPL.), 1223-1228.

[9] X. Zhang, Z. Zhong, H. S. Ruiz, J. Geng, T. A. Coombs, "General approach for the determination of the magneto-angular dependence of the critical current of YBCO coated conductors", Supercond.Sci. Technol., 30(2), 025010(2017)

[10] Lin, B., et al. "Test of Maximum Endurable Quenching Voltage of YBCO-Coated Conductors for Resistive Superconducting Fault Current Limiter." IEEE Transactions on Applied Superconductivity, 2012.

[11] Jin, T., Hong, J., Zheng, H. et al. "Measurement of boiling heat transfer coefficient in liquid nitrogen bath by inverse heat conduction method", J. Zhejiang Univ. Sci. A (2009) 10: 691. https://doi.org/10.1631/jzus.A0820540

[12] Zhang, Min, Koichi Matsuda, and T. A. Coombs. "New application of temperature-dependent modelling of high temperature superconductors: Quench propagation and pulse magnetization." Journal of Applied Physics 112, no. 4 (2012).

[13] Liang, Fei, Weijia Yuan, Carlos A. Baldan, Min Zhang, and Jerika S. Lamas. "Modeling and Experiment of the Current Limiting Performance of a Resistive Superconducting Fault CurrentLimiter in the Experimental System." Journal of Superconductivity and Novel Magnetism 28, no. 9 (2015): 2669-2681.

[14] D. Giancoli, Electric Currents and Resistance, New Jersey: Physics for Scientists and Engineers with Modern Physics 2009.

[15] Manitoba HVDC Research Centre, PSCAD, https://hvdc.ca/pscad/, 2017.

[16] R. Kuffel, J. Giesbrecht, T. Maguire, R. P. Wierckx, and P. McLaren, "RTDS-a fully digital power system simulator operating in real time," in Proceedings of International Conference onEnergy Management and Power Delivery, vol. 2, pp. 498-503, Nov. 21-23, 1995.

[17] 'Simplified 14-Generator Australian Power System', IEEE PES Power System Dynamic Performance Committee available at 'http://eioc.pnnl.gov/benchmark/ieeess/index.htm'

[18] M. Gibbard and D. Vowles, Simplified 14-Generator Model of the SE Australian Power System, Report, Revision 3, 2010.

[19] Infrastructure Security and Energy Restoration Office of Electricity Delivery and Energy Reliability U.S. Department of Energy "Large Power Transformers and the U.S. Electric Grid" June 2012.

[20] Teodorescu, R., Liserre, M., Rodriguez, P., "Grid Converters for Photovoltaic and Wind Power Systems" John Wiley & Sons, Ltd, 2011.